accepted ECS Proceedings, Paris 97
ECS-Proc. Vol. 97-36 (1998) 381-392

UHV-SILICON WAFER BONDING AT ROOM TEMPERATURE: MOLECULAR DYNAMICS AND EXPERIMENTS

Kurt Scheerschmidt, Detlef Conrad, Alexander Belov and Heinz Stenzel

Max Planck Institute of Microstructure Physics, Weinberg 2, D-06120 Halle (Germany)
Fax.: 0345-5511223, Tel.: 0345-5582910, Email: schee@mpi-halle.mpg.de

Silicon wafers bonded under UHV conditions at room temperature are structurally characterized by transmission electron microscopy. The physical processes of wafer bonding and the resulting structure of bonded interfaces are modelled using molecular dynamics simulations. Thus the atomic bonding processes and residual defect structures can be analyzed to better understand the bonding mechanisms.

INTRODUCTION

Classical molecular dynamics (MD) solving the equations of motion of an ensemble of particles provides a tool suitable for simulating time-dependent processes. It is used to investigate the elementary steps of bonding two silicon wafers /1/. Wafer bonding is being widely used in the silicon-on-insulator and micromechanical technology /2/. Its physical processes, however, are not yet well understood. Starting with adhesively bonded materials the covalent interaction of two wafers usually needs some thermal treatment. UHV-experiments, however, demonstrate the possibility of large-area covalent Si wafer bonding at room temperature /3/. Conventional transmission (TEM) and high resolution electron microscope (HREM) structure imaging were applied to investigate the resulting interfaces at an atomic level /3-5/. Bonding energy and forces strongly depend on the surface structure, i.e. roughness, crystallography, native oxides, adsorbates, and hydrophobic or hydrophilic termination, but also on the thermal treatment, the bonding history, and thus the bonding control equipment.

WAFER BONDING

Mirror-polished and smooth pieces of solids adhere to each other provided there are no dust particles between their surfaces. A particle of only about 1μm in diameter causes a bubble of several mm in lateral dimension. To avoid such bubbles a high-quality cleanroom technique of class 10, or better, has to be applied or a special "microcleanroom" /6/ which may be used in basic research. The strength of the adhesion of wafer bonding can be measured by the crack opening technique. Both hydrophilic and hydrophobic wafers bonded in air at room temperature, however, imply rather weak bonding energies (van der Waals forces) of about 0.1 J/m^2,with the bonding being reversible. Covalent bonding yielding high bonding energies ($\approx 2J/m^2$) is attained by annealing the room-temperature bonded wafers at high temperatures ($\geq 1000^oC$). Here the chemistry, morphology, surface roughness, and the annealing time and temperature are the most important factors determining the quality and strength of the bonded interfaces. A typical HREM cross section of bonded hydrophobic (100)-Si-wafers is shown in Fig.1 together with a filtered "lattice fringe" image indicating lattice defects by terminated fringes (Fig. 1b). While the hydrophilic bonded samples are mostly characterized by a thin oxide layer in the interface, the

hydrophobic bonded wafers show different contrast effects at the interface: local stresses, oxide islands, voids, partial dislocation networks due to the mistilt of the wafers, screw dislocation networks due to the rotational misorientation as well as steps and V-shaped stacking faults (see, e.g., /7-9/, where particular configurations are studied in detail /10,11/ for non-Si situations and the more general considerations /12/). While in most of the cases defects reduce the applicability of wafer-bonded devices to microelectronics, the screw dislocation network can be used to grow lattice-mismatched hetero-epitaxial films without threading dislocations /13-15/.

UHV ROOM TEMPERATURE SILICON BONDING

Heat treatments may cause severe problems in wafer bonding, e.g., the formation of interface bubbles by the nucleation of adsorbates etc., or if materials with different thermal expansion are bonded. Thus, for a number of electronically relevant applications as, e.g., bonding after metallization of devices /16/ or including sensitive buried layers /17/, and especially to investigate the physical processes of wafer bonding itself, it is important that the bulk bond strength can be attained by room temperature bonding without any additional heating step. Ultrahigh vacuum (UHV) experiments demonstrated that large-area, self-propagating, room-temperature covalent wafer bonding of commercially available 4" (100) silicon wafers is possible /3/. After the native oxide was removed using hydrofluoric acid, rendering the surfaces hydrophobic and covered with hydrogen, the wafers were bonded as usual in a microcleanroom. In the UHV-chamber, the bonded wafers were separated, and the hydrogen was removed by heating and pumping. After cooling to room temperature, within the UHV-chamber the bonding was initiated by an appropriate manipulator in the centre of the wafer. Figure 2 shows an infrared image of the in situ UHV bonding process, the light gray area marks the bonded region. Mechanical tests showed that the wafers were covalently bonded. Similar results were obtained for larger wafers, additionally applying surface activation and/or pressure and low-temperature annealing to enhance the bonding process /18-22/. Figure 3 shows the resulting structure, viz. the example of an interface of room-temperature UHV-bonded silicon wafers investigated by cross-sectional HREM (Fig. 3a, 200kV, [110] orientation). Though not showing any noticeable intermediate layer and being flat the interface does not correspond to a perfect structure. Along the interface darker diffraction contrast regions occur at distances of about 5-7 nm. This may be due to incomplete bonding processes arising from misorientations of the two wafers, fast energy dissipation, or defects left behind at surface structures as, e.g., at surface steps. The corresponding images filtered of the selection marked (Fig. 3b: "lattice fringe images" of reflection pairs 111 and 002) show additional lattice planes indicating interfacial dislocations. Figure 3c shows a plan-view TEM image of the same UHV room-temperature bonded wafers, demonstrating that large regions are well bonded creating a screw dislocation network to fit the rotational misorientation of about 1.3^{o}, similarly to the results generally obtained for hydrophobically bonded wafers after a high temperature treatment /8,9,12,14/. Additional defects arise probably due to an incomplete bonding at surface terraces or steps. For comparison, simulated HREM and TEM images of bonded interfaces with steps or rotational misfit are given in Figs. 5- 8, calculated by MD modelling, which will be discussed in detail later on.

MOLECULAR DYNAMICS SIMULATIONS

The MD simulation of macroscopically relevant structures requires a large number of particles to be considered and many-body empirical potentials to be applied, which should be in agreement with ab initio calculations and covering bulk and surface structures as well

as the interaction with adsorbates, etc. The interatomic forces in covalent solids can completely be described only if the influence of the local environment according to the quantum electronic structure is also included. However, empirical potentials have been developed, which allows one to simulate the non-local many-body interaction sufficiently well, thus enabling the application of long-time MD simulations to larger systems as it is necessary to investigate, e.g., the wafer bonding interaction processes. The potential of Tersoff predicts the asymmetric reconstruction with fourfold coordinated atoms at interfaces with defects. Therefore it was applied to investigate the cores of 60° partial dislocations in Si and other defects left after bonding two wafers /23,24/. Because of the short range of the Tersoff potential it was supposed here that the bond topology is given by the usual process starting with separated Si blocks of suitable surface structure and orientation (surface reconstruction, steps and adsorbates) and applying long-range potentials. The potential most often used for group IV semiconductors is the Stillinger-Weber potential, with a smooth cut-off behind the nearest neighbour distance, and which is scaled with respect to the cohesive energy, the lattice constant, and the melting point. In contrast to the Tersoff potential it supports a symmetric quasi-fivefold coordinated reconstruction at interfaces /23/. The Stillinger-Weber potential, however, allows the next neighbour interaction to be included, which is a presupposition to the simulation of the dynamical behaviour without preordered surfaces and prescribed topology. The interaction of two silicon surfaces can be studied solely by correctly revealing the 2x1 reconstruction of a clean Si(100) surface. Thus as a first improvement, the potential has to be rescaled to the next neighbour interaction generating almost instantaneously a fully symmetrically dimerized surface within a few 100 femto seconds, and showing energy gain and bond length in good agreement with ab initio results /1/. The second improvement is related to the energy transfer, because each new bond implies an energy gain of the order of eV, which in a constant energy simulation (NEV-ensemble) is distributed to a small number of atoms resulting in an inappropriate melt of the surfaces. The energy dissipation and thus the dynamic bonding behaviour are controlled by the transfer rates of the kinetic energy at the borders of the model describing an energy flux into a macroscopic substrate, thus enabling an energy minimization. Two approaches are applied to rescale the averaged velocities of the outermost atomic layers every 100 time steps either down to a constant temperature (fast heat transfer), or by using a constant reduction factor (slow heat transfer). A more frequent rescaling would affect the lattice vibrations. Within the fast heat transfer approach, the average kinetic energy at the borders of the simulated system remains constant whereas within the slow heat conduction the flux is controlled such that the temperature far away from the interface remains constant. The molecular dynamics simulation starting with two perfect and parallel-oriented Si blocks with perfectly aligned 2x1 reconstructed (100) surfaces and applying a slow heat transfer approach yields perfect bonding /1/. However, a fast heat transfer, a starting configuration, with the dimer rows in orthogonal domain orientation, or including steps etc. as discussed in the following, will result in configurations no longer perfectly coordinated /1,4,5,23,24/. Additionally, the heat flux should be treated as a nonequilibrium or a nonholonom problem and the system should be coupled elastically to the bulk wafers. Following text books a heat-bath may be described with Gaussian minimum constraints and the coupling of the elastic field is possible via Lagrange parameters similar to a Nose-Hoover thermostat or an Anderson mechanic. The MD simulations of defects considered here result in slightly changed structures and energies as will be reported elsewhere.

STEPS AND VICINAL INTERFACES

Studying the energy flux at surfaces with atomic steps (see Fig. 4) allows one to investigate the restrictions on the bonding process of more realistic surfaces, which are vicinal.

In Fig. 4, the grey level describes the potential energy above the ground state, which is dark. The upper terraces behave like perfect surfaces (Fig. 4a): Starting with dimerized surfaces, a weak attraction owing to the next neighbour interaction initiates the dimers to rearrange and to create new bonds. The energy the bonds have gained dissipates (Fig. 4b) increasing the kinetic and elastic energies of the bulk. If the heat transfer is slow enough, the resulting avalanche effect implies the bonding of the lower terraces, too. However, after relaxation defects are left resembling dissociated partial dislocations (cf. Fig. 4c). Figure 5 shows a simulated defocus series of the metastable double-layer step according to Fig. 4c, i.e. the symmetric, metastable, quasi-fivefold coordinated reconstruction. Both the HREM images and the filtered "lattice fringe" images demonstrate the strong influence of the imaging conditions on the contrast details obtained.

The slow heat simulation by a Tersoff potential allows further relaxation: a double-layer step does not change the dimer orientation and may finally relax to 60° partial dislocations (see Fig. 6a, upper row) possibly associated with a row of vacancies depending on the barriers to rigid-body translations between the steps. In contrast to that, single layer steps rotate the dimerization direction in the neighbouring domains, thus giving rise to a stacking fault (see Figs. 6 b,c, upper row, of interstitial and vacancy type, resp.) of 90° twist rotation, i.e. a fourfold screw axis. Further relaxation applying the Tersoff potential to single layer steps results in an asymmetric interface with fourfold coordinated atoms, which can be imagined to consist of arrays of a new structural unit, the 42m-dreidl: 14 atoms in 8 five-membered rings /23,24/. HREM images of the (100) intrinsic and extrinsic stacking faults (Figs. 6b and c, resp.) as well as the fully relaxed 60° partial dislocations with rows of vacancies (Fig. 6a) are simulated for the Gauss-focus (Δ=0) and the underfocus of Δ=100nm. These images and the corresponding filtered "lattice fringe" micrographs demonstrate that the effect of the (2x2) reconstruction on the image contrast (a double contrast periodicity with respect to the perfect lattice contrast) can be enhanced, or suppressed by choosing the appropriate defocus values. The contrast details and the analysis of terminated fringes in all reflections of filtered images, or in diffraction contrast allow one to discriminate the different defects in Figs. 5 and 6.

TWIST WAFER BONDING

To study the effect of a small twist angle (cf. Fig. 7), one surface is rotated by an angle of 4.6° corresponding to a Σ=313 boundary /1/. Fig. 7a shows a plan view of the starting configuration. With the surfaces closely approaching and bonds forming in between (with respect to an appropriate cut-off radius), at the beginning there are three distinct regions at the interfaces in which the dimer rows of the upper surface lie in between those of the lower one, or on top of each other, or having a bulk-like environment. After sufficient relaxation under slow heat transfer conditions almost all atoms have a bulk-like environment as the final state in Fig. 7b indicates, viz. those regions are separated by misfit dislocations, which possibly have a high rate of kinks. Fig. 7c shows the simulated 400 kV HREM images of the bonded interface of Fig. 7b for different defoci. In 110-direction, a fringe contrast occurs agreeing with the experimental observations: columns of atom pairs periodically disturbed by the diffraction contrast due to elastic strain. However, for all defocus values chosen additional fringes do not directly occur. Image filtering shows additional fringes solely parallel to the interfaces, probably because the model is too small for correct image calculations. The effect of the small twist angle as a rotational misorientation without other defects can also be described as a mosaic-like interface structure consisting of a screw dislocation network. This structure can directly be imaged by EM plan-view

diffraction contrast as shown by image simulations in Fig. 8 based on the MD model of Fig. 7c. The resulting diffraction contrast is analyzed for different imaging conditions: thicknesses of 4.3, 8.6 and 12.9nm; objective apertures of 2, 3.5 and 5 nm^{-1}; beam orientations according to the excited reflections 000, 400, etc. The network can clearly be revealed under all conditions chosen. Besides dark contrast regions occur due to local bendings of the lattice planes indicating the tilt, and moire fringes superimposed for thicker crystal slabs (cf. experiments above).

HYDROGENATED SURFACES

The influence of adsorbates is investigated for hydrogenated surfaces assuming two Si(001)-3x1 blocks, corresponding to a hydrogen coverage of 4/3 monolayers. The calculations were performed for a NVT-Ensemble at 300K (336 Si, 64 H atoms), with periodic boundary conditions applied solely to the directions parallel to the surfaces /25/. Starting with a separation below the cut-off range of the additionally applied hydrogen-hydrogen interactions, the distance of the surfaces increases due to the strong repulsive forces of the hydrogen atoms and the van der Waals interactions being neglected. External forces in the direction perpendicular to the interface are added to the interatomic forces of the two outermost atomic layers of each slab. A time step of 0.12fs is used to account for the fast dynamics of the hydrogen atoms. Fig. 9 shows the distance of the surfaces vs the simulation time for different external forces applied. The distance measured is the difference of the average z-coordinates of the uppermost and the lowest atomic layers of the whole model, subtracting the thickness of a perfect Si crystal with the same number of atomic layers, thus including also bond breaking and rearrangements at the interface. Under the weak external stress of about 13.5 MPa, the surfaces approach each other, with the repulsion causing an oscillatory behaviour. With external forces increasing as, e.g. at a stress of 27 MPa (cf. Fig. 9), the time average distance of the surfaces decreases. For an external force of 54MPa, the silicon atoms of one surface may interact with the hydrogen atoms of the opposite surface, causing a weak attraction of the surfaces. With the external forces ranging between 54 MPa and 81 MPa, the distance of the surfaces varies only slightly and different ordering of the hydrogen atoms between the silicon surfaces occuring. Removing the external forces and continuing the calculation for another 10^5 time steps, result in a weak relaxation, but no separation of the surfaces, indicating that adhesion takes place, instead of a dynamic equilibrium. Further increasing the external forces causes the number of silicon-silicon interactions to increase between the distorted surface layers, and a further decrease of the distance smaller than that of an equivalent perfect Si crystal. As a consequence, hydrogen atoms desorb from the surface, being able to diffuse into the crystals or, more likely, along the interface. However, besides the deformations directly at the interface and some hydrogen interstitials, there are no additional defects created in the bulk, since the forces are smaller than the theoretical shear stress of about 40 GPa, and the critical force is much smaller than the Peierls stress of about 4 GPa. However, for comparing the predicted forces with results from experiments still to be performed needs some rescaling to include the effects of the empirical potentials, the boundary conditions as well as the restricted size of the model.

CONCLUSIONS

Molecular dynamics simulations based on empirical potentials were used to investigate the elementary steps of bonding two Si(001) wafers. The resulting interface models were applied to analyze high resolution electron microscopy structure images. Bonded structures including surface steps were additionally refined by simulating the relaxation through em-

pirical Tersoff potentials. The applicability of the method was demonstrated by studying the interaction of wafer surfaces without adsorbates, which corresponds to UHV bonding conditions. Calculations covering the influence of surface steps, rotational misorientations and adsorbates were carried out to correlate atomic properties with macroscopic ones. For adsorbate-free, perfectly aligned surfaces, which were twisted by 90^{o} as, e.g., at monoatomic steps, the most stable configurations shows a new type of structural unit. Depending on the type of reconstruction and the energy transfer, expansion or contraction of bonds as well as metastable configurations are obtained. For a non-restricted relaxation, the boundaries tend to optimize the angular bond distortions because the most important factor is the directionality of the bonds. MD simulations showed that the most crucial problem consists in finding complex atomic potentials covering bulk and surface structures as well as the interaction with adsorbates, etc. Finally, the resulting bonding energy depends on the assumptions of the molecular dynamics modelling as, e.g., heat transfer, elastic coupling, and neglecting weak long-range interactions.

REFERENCES

1. D. Conrad, K. Scheerschmidt and U. Gösele, Appl. Phys. **A 62**, 7 (1996).
2. U.M. Gösele, M. Reiche and Q.Y. Tong, Proc. 4th Intern. Conf. Solid-State and Integrated Circuit Technology, Beijing, China 1995. Eds: G.L. Baldwin, et al., New York, USA: IEEE, 1995, p.243.
3. U. Gösele, H. Stenzel, T. Martini, J. Steinkirchner, D. Conrad and K. Scheerschmidt, Appl. Phys. Lett. **67**, 3614 (1995).
4. K. Scheerschmidt, D. Conrad and U. Gösele, Comput. Mater. Sci. **7**, 40 (1996).
5. K. Scheerschmidt, D. Conrad, A.Y. Belov and U. Gösele, Comput. Mater. Sci. (1997) in print.
6. R. Stengl, K.-Y. Ahn and U. Gösele, Jpn. J. Appl. Phys **27**, L2364 (1988).
7. M. Reiche, K. Scheerschmidt, D. Conrad, A. Belov, U. Gösele, K.N. Tu, Inst. Phys. Conf. Ser. (1997) in print.
8. M. Benamara, A. Rocher, P. Sopena, A. Claverie, A. Laporte, G. Sarrabayrousse, L. Lescouzeres, A. Peyre-Lavigne, Materials Science & Engineering **B42**, 164 (1996).
9. A. Laporte, M. Benamara, G. Sarrabayrousse, A. Rocher, L. Lescouzeres, A. Peyre-Lavigne, A. Claverie, Electrochem. Soc. Proc. **95-7**, 342 (1995).
10. G. Patriarche, F. Jeannes, F. Glas and J.L. Oudar, Inst. Phys. Conf. Ser. **146**, 409 (1995).
11. R.J. Ram, J.J. Dudley, J.E. Bowers, L. Yang, K. Carey, S.J. Rosner and K. Nauka, J. Appl. Phys. **78**, 4227 (1995).
12. R. Gafiteanu, S. Chevacharoenkul, U. Gösele and T.Y. Tan, Inst. Phys. Conf. Ser. **134**, 87 (1993).
13. F.E. Ejeckam, Y.H. Lo, S. Subramanian, H.Q. Haou and N.M. Jokerst, Appl. Phys. Lett. **70**, 1754 (1997).
14. T.Y. Tan and U. Gösele, Appl. Phys. **A64**, 631 (1997).
15. N. Sato, K. Sakaguchi, K. Yamagata, Y. Fujiyama, J. Nakayama and T. Yonehara, Jpn. J. Appl. Phys. **35**, 937 (1996).
16. A.Q. Huang, IEEE Trans. Electron Devices **43**, 1029 (1996).
17. K. Ljungberg, A. Söderbärg, S. Bengtsson and A. Jauhiainen, J. Electrochem. Soc. **141**, 562 (1994).
18. R. W. Bower and F. J. Y. Chin, Jpn. J. Appl. Phys. Lett. **36**, L527 (1997).
19. H. Takagi, K. Kikuchi, R. Maeda, T.R. Chung and T. Suga, Appl. Phys. Lett. **68**, 2222 (1996).
20. K. Ljungberg, F. Grey and S. Bengtsson, Appl. Surface Science **117**, 105 (1997).
21. S.N. Farrens, J.R. Dekker, J.K. Smith and B.E. Roberds, J. Electrochem. Soc. **142**, 3949 (1995)
22. T.R. Chung, L. Yang, N. Hosoda and T. Suga, Nuclear Instruments & Methods in Physics Research, **B121**, 203 (1997).
23. A.Y.Belov, D. Conrad, K. Scheerschmidt and U.Gösele, Phil. Mag. Letters (1997) in print .
24. A.Y. Belov, D. Conrad, K. Scheerschmidt and U. Gösele, Inst. Phys. Conf. Ser. (1997) in print.
25. D. Conrad, K. Scheerschmidt and U. Gösele, Appl. Phys. Letters (1997) in print.

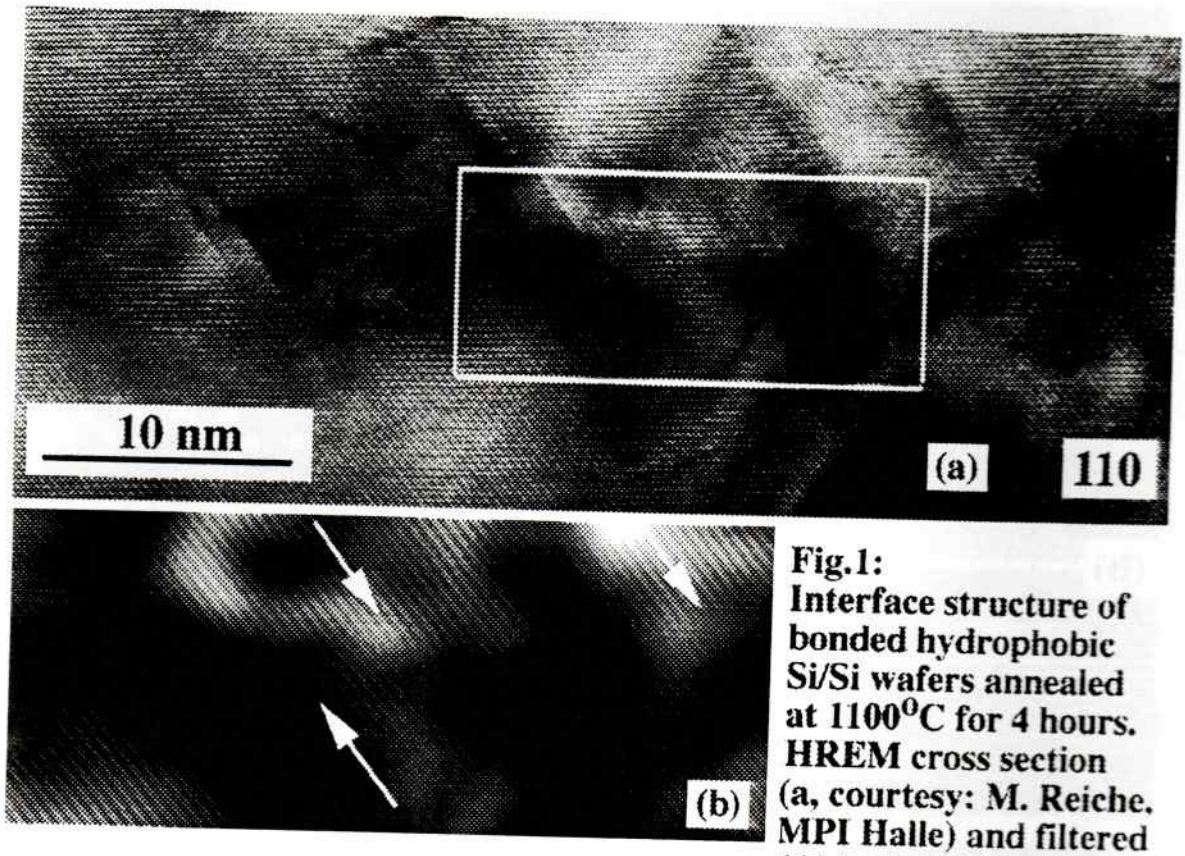

Fig.1:
Interface structure of bonded hydrophobic Si/Si wafers annealed at 1100°C for 4 hours. HREM cross section (a, courtesy: M. Reiche, MPI Halle) and filtered 111-lattice fringes (b).

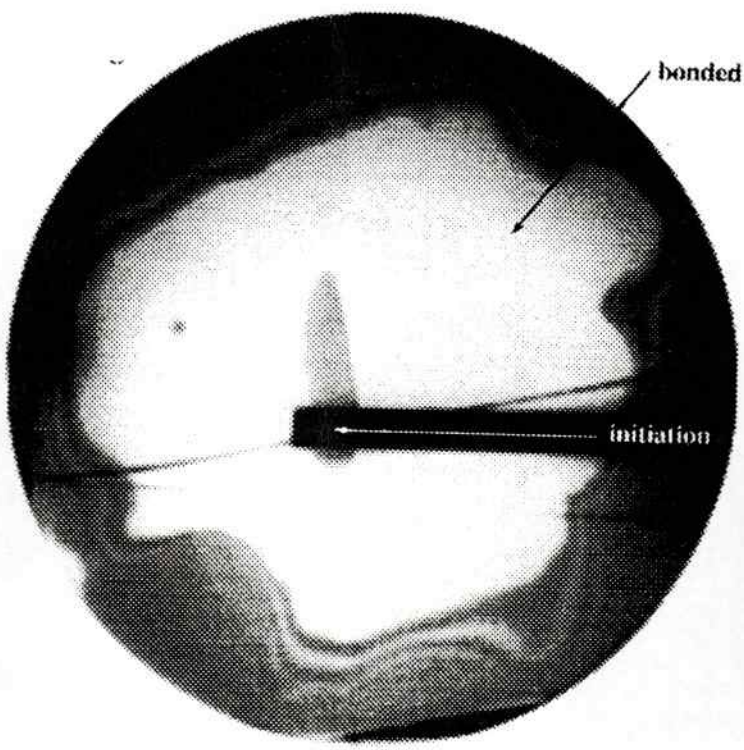

Fig.2:
Infrared transmission image (in situ) of room-temperature UHV bonded silicon wafers (bright areas correspond to self-propagating bond wave; 4 inch wafer; 100-orientation)

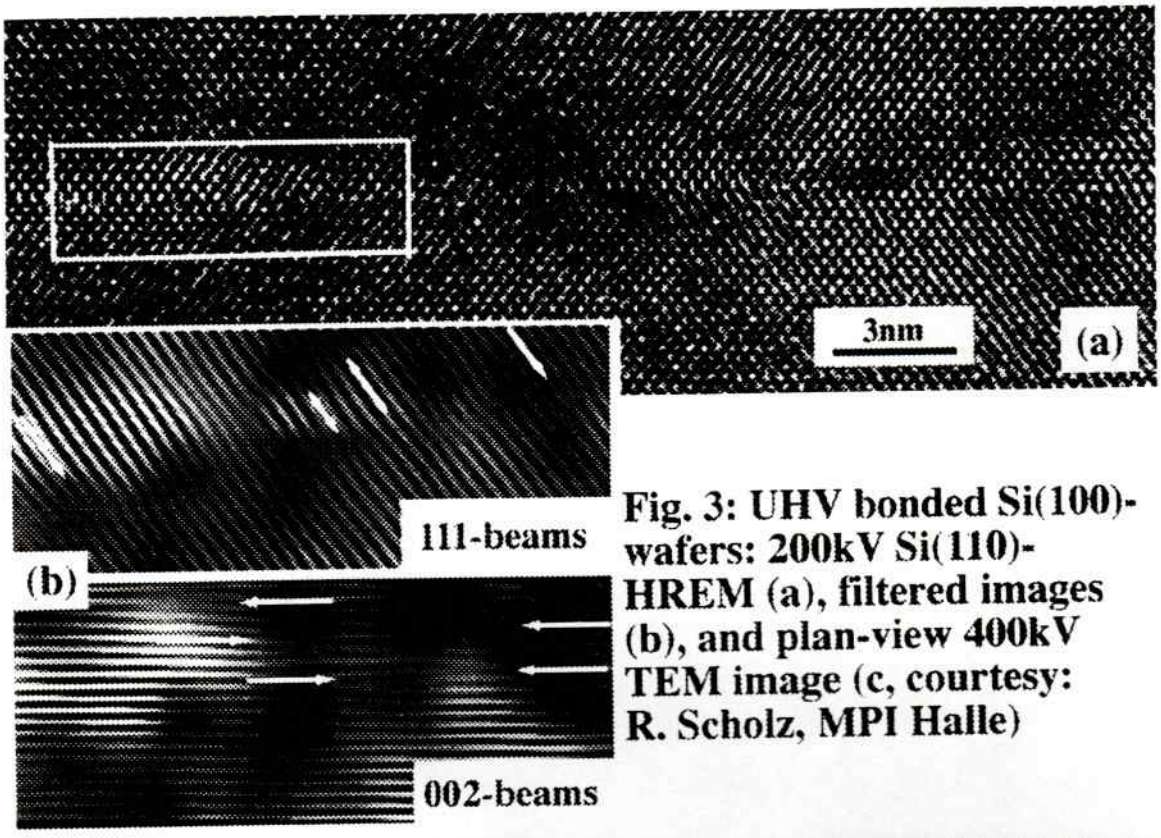

Fig. 3: UHV bonded Si(100)-wafers: 200kV Si(110)-HREM (a), filtered images (b), and plan-view 400kV TEM image (c, courtesy: R. Scholz, MPI Halle)

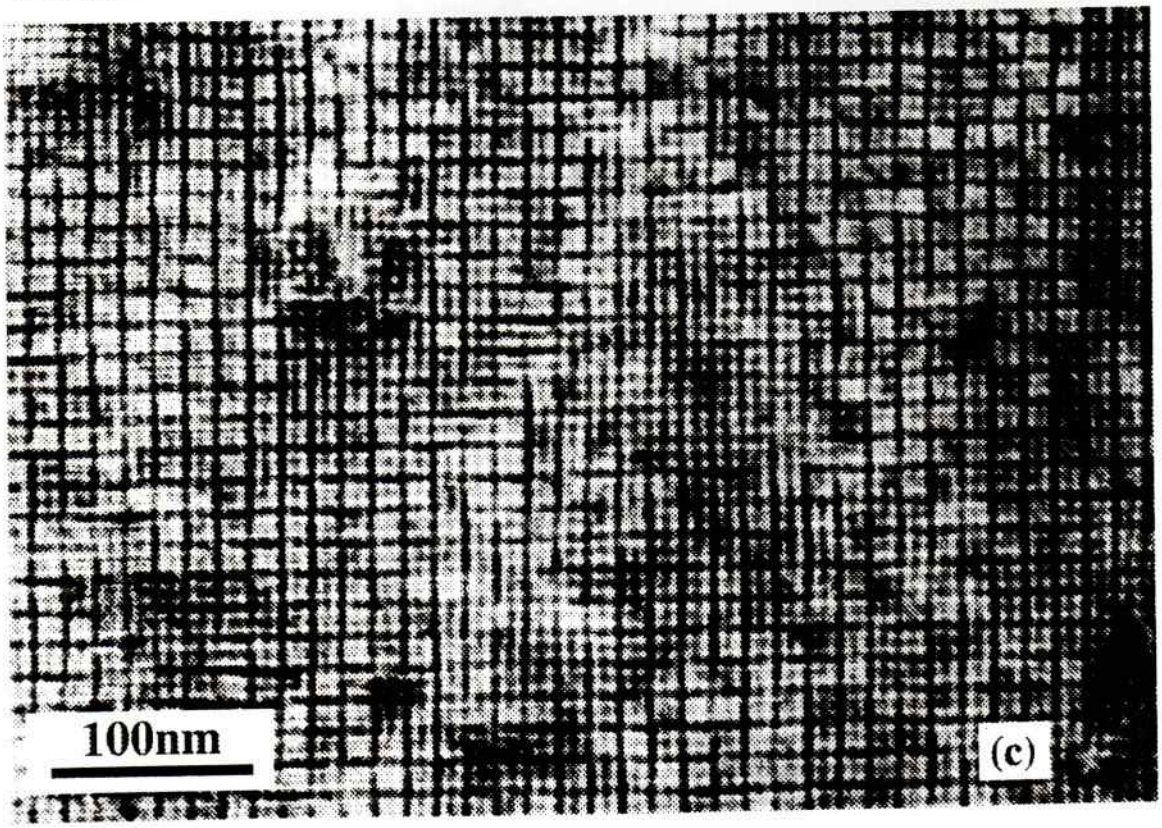

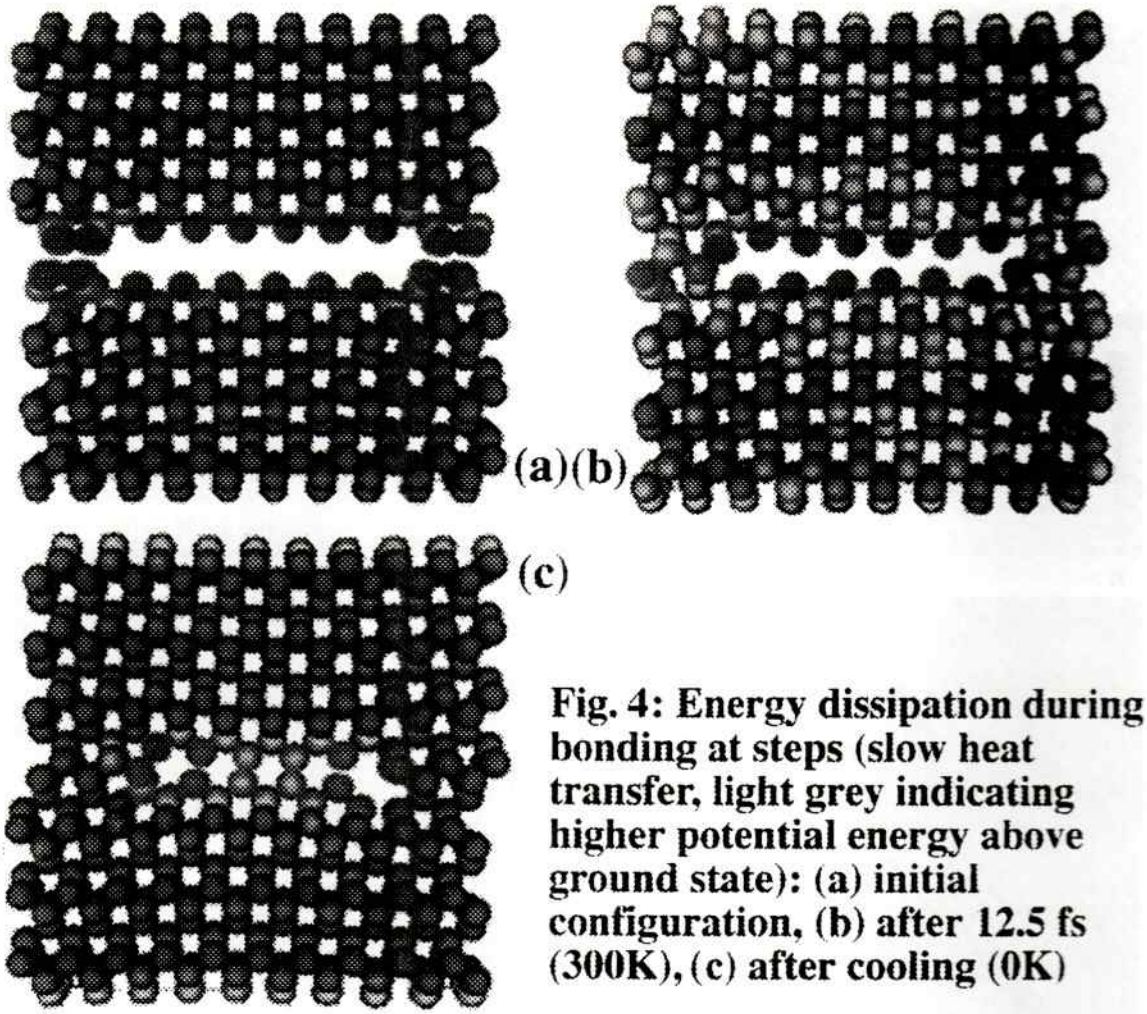

Fig. 4: Energy dissipation during bonding at steps (slow heat transfer, light grey indicating higher potential energy above ground state): (a) initial configuration, (b) after 12.5 fs (300K), (c) after cooling (0K)

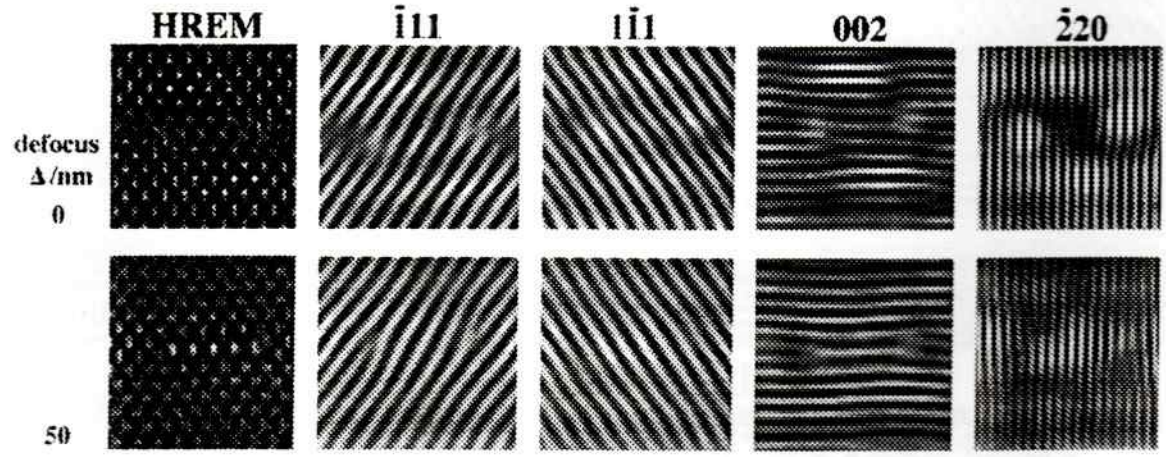

Fig. 5: MD simulated (001)-Si wafer bonding at double steps: theoretical 200kV-[110]-HREM and filtered images (spherical aberration=1mm, defocus spread=1nm, beam divergence=.05mrad, thickness=7.9nm)

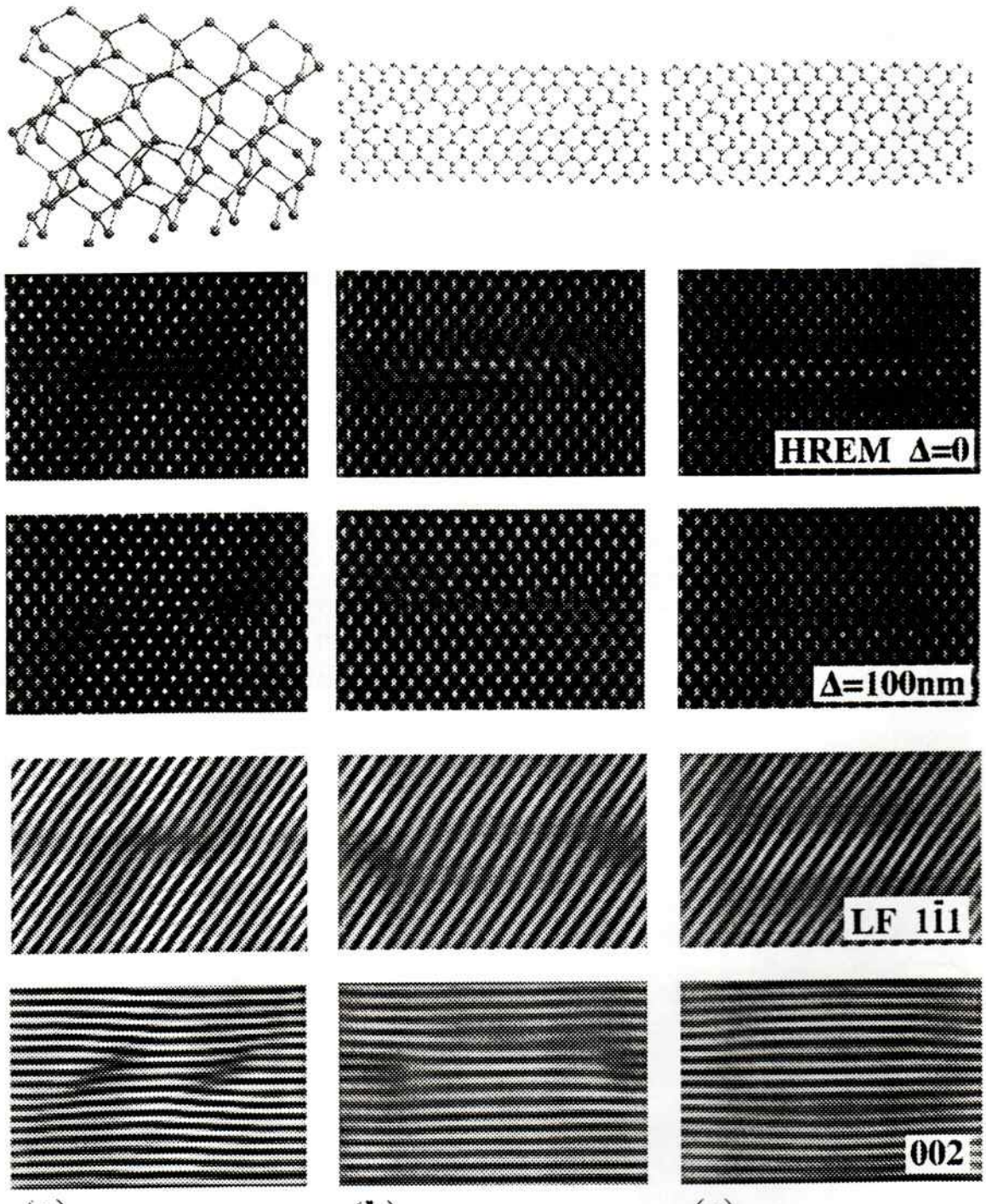

Fig. 6: Simulated 200kV-[110] HREM and filtered LF images (thickness = 6.1nm, defocus Δ):
(a) dislocation with line of vacancies (double step),
(b) intrinsic, (c) extrinsic stacking faults (single steps)

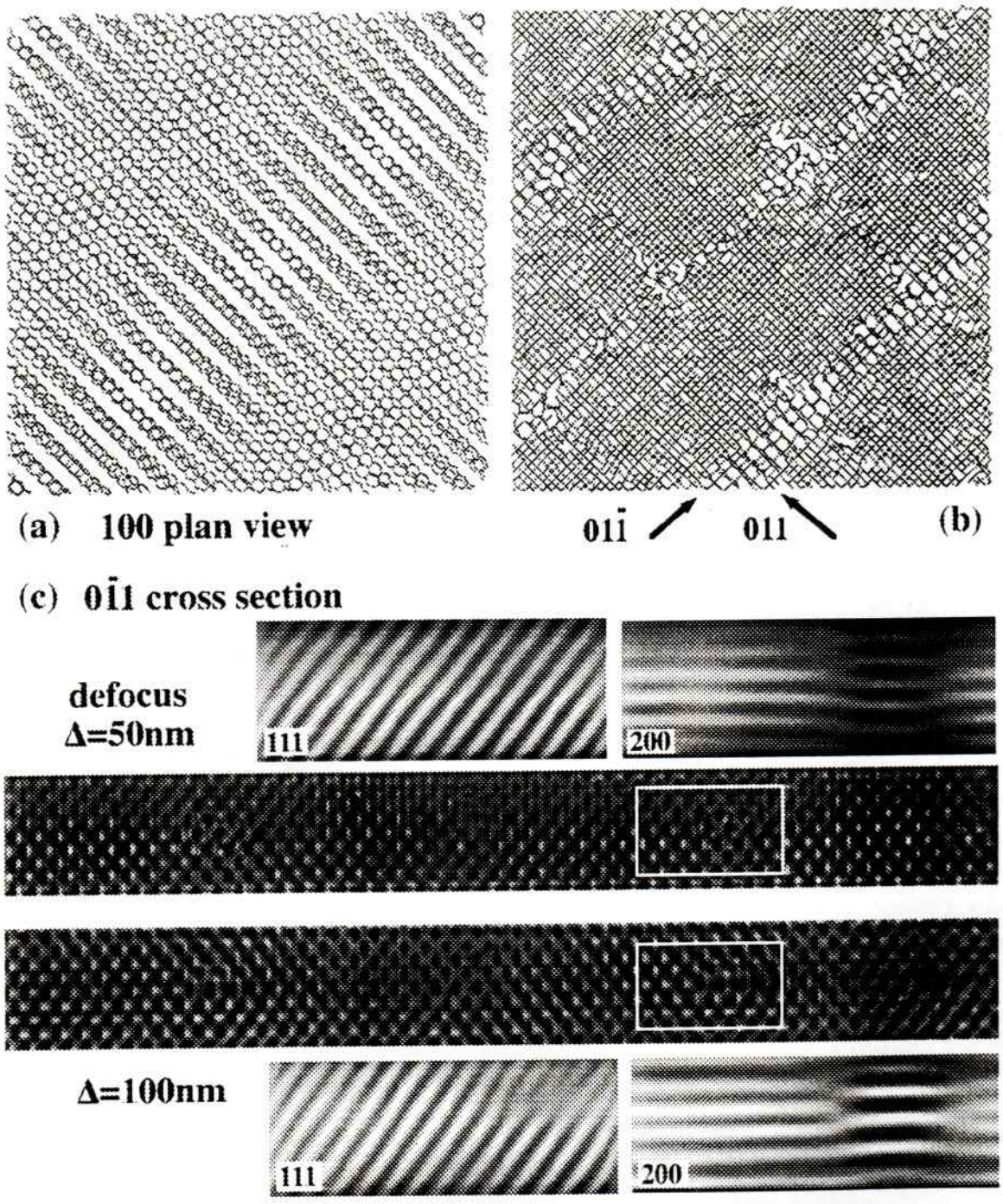

Fig. 7: Si(100) wafer bonding with rotational misorientation $\Sigma 313(4.6^{o})$ before (a) and after MD-relaxation (b, 1.25ps 300K, 1.25ps 900K); Simulated 400kV HREM micrographs and filtered selections (c, from 0$\bar{1}$1 of b, spherical aberration=1mm, defocus spread=8nm)

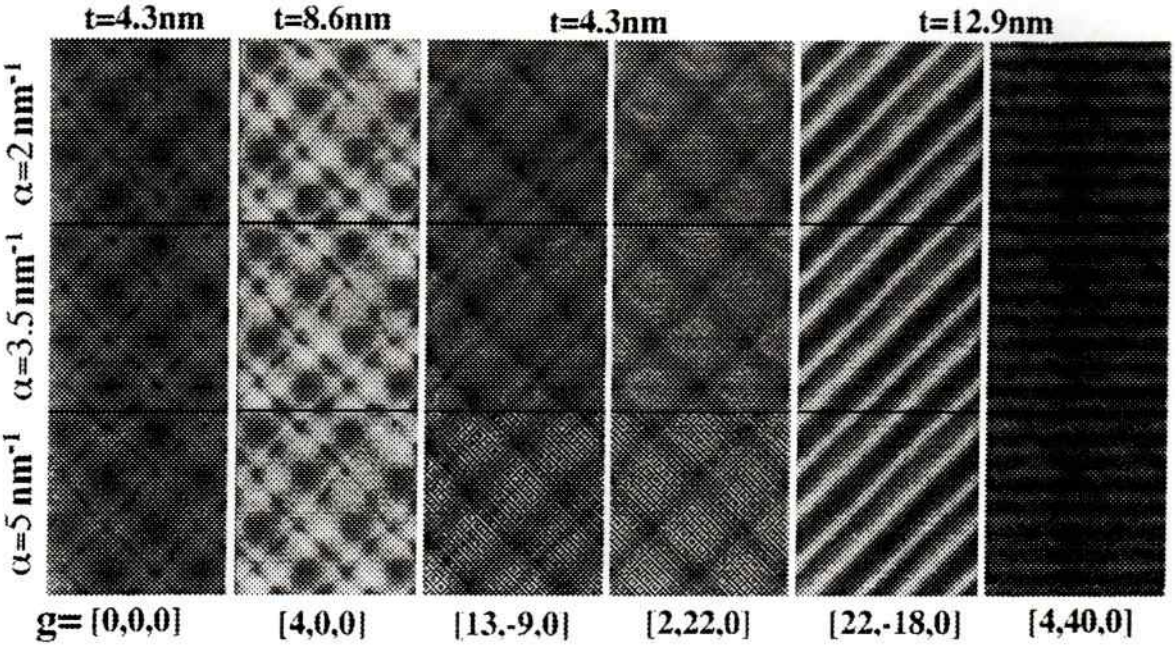

Fig. 8: Simulated 200 kV plan-view TEM micrographs as function of thickness t, objective aperture α, and excited reflections g : MD-relaxed Si(100) wafer bonding with 4.6° misorientation

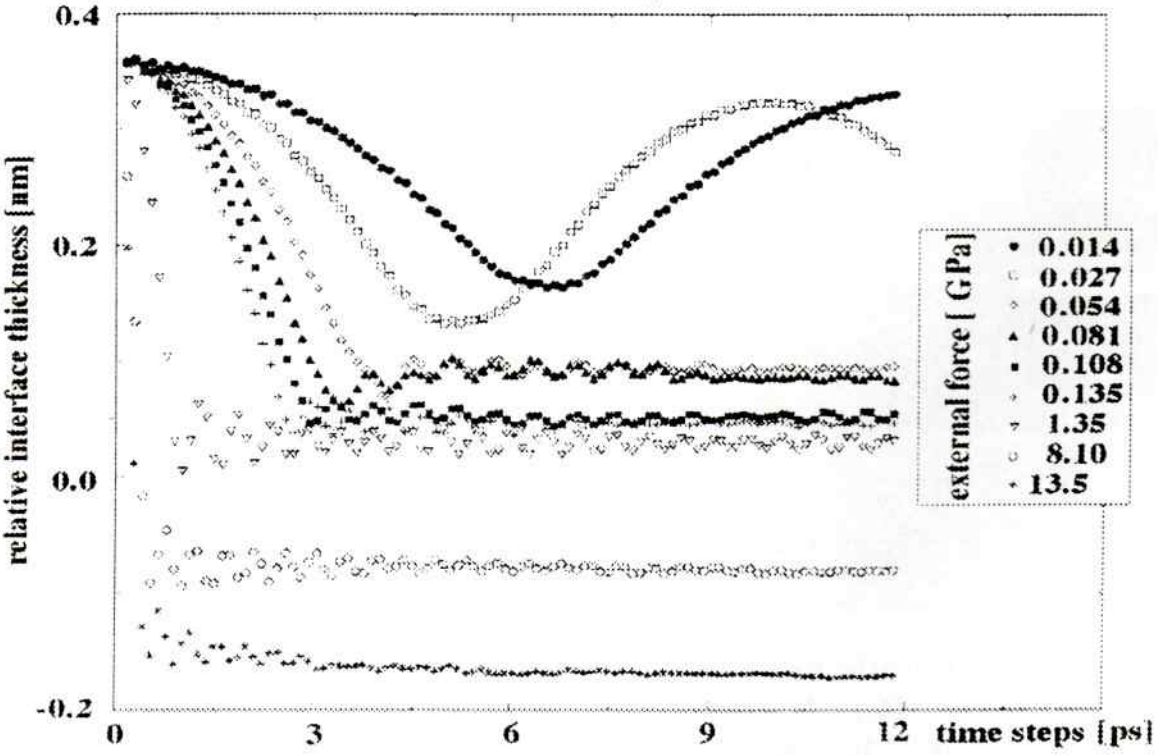

Fig. 9: Equilibrium distances of hydrogenated Si surfaces as a function of the MD simulation time for different external forces applied